JOURNAL OF GEOPHYSICAL RESEARCH: OCEANS, VOL. 118, 619–634, doi:10.1029/2012JC008306, 2013

A two-phase model for sheet flow regime based on dense granular flow rheology

T. Revil-Baudard[1] and J. Chauchat[1]

Received 21 June 2012; revised 26 November 2012; accepted 3 December 2012; published 4 February 2013.

[1] A two-phase model having a $\mu(I)$ rheology for the intergranular stresses and a mixing length approach for the turbulent stresses is proposed to describe the sheet flow regime of sediment transport. In the model, two layers are considered: a dilute suspension layer and a dense sediment bed layer. The concentration profile is obtained from the dilatancy law $\phi(I)$ in the sediment bed layer and from a Rouse profile in the suspension layer. The comparison of velocity profile, concentration profile, and macroscopic parameters (sediment transport rate, thickness, and roughness) with experimental data shows a good agreement. These comparisons demonstrate that the dense granular rheology is relevant to describe intense bed-load transport in turbulent regime (sheet flow). The transition from the dense static bed to the dilute suspension is well described by the present model. Also, the different regimes of the dense granular rheology seems to be able to capture the transition between collision-dominant and turbulent-fluctuations-dominant sheet flows, depending on the particle's characteristics.

Citation: Revil-Baudard, T., and J. Chauchat (2013), A two-phase model for sheet flow regime based on dense granular flow rheology, *J. Geophys. Res. Oceans*, *118*, 619–634, doi:10.1029/2012JC008306.

1. Introduction

[2] The sheet flow regime of sediment transport is associated with extreme events such as sandstorms, river floods, or storm waves in the surf zone. Because of the huge amount of sediment transported in this regime, it is especially important for the understanding of the morphological evolution and the stability of constructions in riverine and coastal environments.

[3] From a physical point of view, the sheet flow regime is characterized by a high bed shear stress [e.g., *Hanes and Bowen*, 1985] represented by the so-called Shields number θ—the ratio of the force exerted by the fluid on the sediment bed over the apparent weight of a single particle. It is usually considered that sheet flow occurs for a Shields number higher than 0.5, which corresponds to roughly 10 times the critical Shields number θ_c in the turbulent regime. The flow is strong enough to wash out bedforms; the sediment bed becomes flat and the thickness of the bed-load layer δ_s is of order of 10 times the particle's size d_p. It is widely accepted that particle-particle interactions, such as collisions and frictional interactions, and fluid turbulent velocity fluctuations are the key mechanisms controlling the sheet flow (*Bagnold* [1956] and *Jenkins and Hanes* [1998] among others).

[4] In this paper, we focus on uniform steady sheet flows. Such sheet flow conditions have been studied in small-scale experiments by *Wilson* [1966, 1989], *Nnadi and Wilson* [1992], *Sumer et al.* [1996], *Gao* [2008], and *Cowen et al.* [2010]. In these studies, velocity and concentration measurements and image analyses were performed for different sediment types and different flow conditions.

[5] The first attempts in modeling sheet flow were conducted by *Hanes and Bowen* [1985] and *Wilson* [1987], among others. In these models, the concentration profile is prescribed and the intergranular stresses are given by a phenomenological law [e.g., *Bagnold*, 1954]. Over the past 15 years, two-phase models, based on kinetic theory of granular flows to describe intergranular stresses, have been applied with some success to model the sheet flow regime [e.g., *Jenkins and Hanes*, 1998; *Greimann and Holly*, 2001; *Hsu et al.*, 2004; *Longo*, 2005; *Amoudry et al.*, 2008]. In these models, the kinetic theory has been stated for situations in which collisional interactions are the dominant mechanism of momentum transfer. The concentration profile is obtained from a balance between collisional interactions and gravity as a result of the model. The collisional shear stresses are linked to the strength of the particle velocity fluctuations represented by the granular temperature. For this new variable, an equation for energy conservation has to be solved with complex boundary conditions in addition to the momentum conservation equation for the particulate phase. *Berzi* [2011] has proposed a simplified analytical solution for the collisional sheet flow regime based on a layer decomposition: a collisional layer based on the kinetic theory of granular flows and a macroviscous layer describing the transition from the collisional regime to the quasi-static one (i.e., fixed bed). This last layer is introduced to circumvent one of the main

[1]Laboratoire des Ecoulements, Géophysiques et Industriels, UMR 5519, UJF, INPG, Grenoble, France.

Corresponding author: J. Chauchat, Laboratoire des Ecoulements, Géophysiques et Industriels, UMR 5519, UJF, INPG, Grenoble, France. (julien.chauchat@grenoble-inp.fr)

© 2012 American Geophysical Union. All Rights Reserved.
2169-9275/13/2012JC008306

limitations of the kinetic theory of granular flows, the modeling of repeated collisions and/or enduring contacts [*Jenkins*, 2006].

[6] Recent improvements in the understanding of the liquid regime of dense granular flows [*GDR midi*, 2004; *Cassar et al*., 2005; *Forterre and Pouliquen*, 2008; *Boyer et al*., 2011] has led to the proposition of a viscoplastic rheology. This rheology exhibits a threshold of motion, controlled by the static friction coefficient and the particulate pressure, and a shear rate dependence of the particulate shear stress characteristic of a viscous-like behavior. It has been used with some success by *Ouriemi et al*. [2009] and *Aussillous et al*. [2012] to model bed-load transport in laminar shearing flows. The author's two-phase model is based on the phenomenological granular rheology $\mu(I)$ for the intergranular stresses [*Forterre and Pouliquen*, 2008]. The concentration profile is either assumed constant in the moving sediment layer or obtained from the $\phi(I)$ phenomenological law [*Boyer et al*., 2011].

[7] The phenomenological laws $\mu(I)/\phi(I)$ are based on dimensional analysis where I represents the dimensionless number controlling the friction coefficient μ and the volume fraction ϕ [*Forterre and Pouliquen*, 2008]. It can be interpreted as the ratio of a vertical time scale of rearrangement to a horizontal time scale of deformation. When the deformation time scale is large (small shear rate) compared with the time scale of rearrangement, the granular media is in the quasi-static regime ($I << 1$). When the parameter I is of order unity ($I \approx 1$), the granular media is in the liquid regime of dense granular flows. In this regime, the concentration ϕ decreases and the friction coefficient μ increases with the dimensionless number I. When the parameter I is much greater than unity ($I >> 1$), the granular media is in the gaseous regime.

[8] Following *Courrech du Pont et al*. [2003] and *Cassar et al*. [2005], three regimes can be observed for the vertical time scale of rearrangement: free fall, viscous, or turbulent, leading to the three corresponding regimes for the phenomenological rheology. The dry granular case pertains to the free-fall regime and has been extensively studied over the last two decades [e.g., *Forterre and Pouliquen*, 2008, and references therein]. In the viscous regime, *Boyer et al*. [2011] have proposed relationships for the two constitutive laws $\mu(I)$ and $\phi(I)$ based on annular shear cell experiments. These relationships are valid in the range $\phi \in [0.3;0.585]$ for spheres.

[9] In this paper, a two-phase model for turbulent flows inspired from the early work of *Ouriemi et al*. [2009] and *Aussillous et al*. [2012] in the laminar case is presented. In the turbulent case the concentration decreases continuously from the static bed up to the suspension [*Nnadi and Wilson*, 1992; *Sumer et al*., 1996]. The phenomenological laws $\mu(I)/\phi(I)$ are used to account for the intergranular stresses and the dilatancy effects inside the sediment bed layer. In the suspension a Rouse profile is assumed to represent the suspended sediment transport. As a first step a simple mixing-length model is used to model the fluid Reynolds stresses. The main objective of the present contribution is to propose an alternative approach to the kinetic theory of granular flows to describe the intergranular stresses based on the dense granular flow rheology for the modeling of sheet flow regime. The velocity and concentration profiles predicted by the present model are compared to existing experimental data from the literature. The evolution of the sediment transport rate, the moving sediment layer thickness, and the equivalent roughness are compared to empirical correlations and available experimental data for a wide range of Shields number. Modeling of transitions from the dense static bed to the dilute suspension and between collision-dominant and turbulent-fluctuations-dominant sheet flows are also investigated in the present work.

[10] The model formulation and numerical algorithm are presented in section 2. The results are presented in section 3, while section 4 is dedicated to the discussion.

2. Model Formulation

[11] A sketch of the flow is presented in Figure 1. The domain is decomposed into two layers: a fluid layer (FL) and a sediment bed layer (SBL).

[12] In the FL, the turbulent fluid flow is driven by gravity and exerts a shear stress on the SBL. In the SBL, the fluid-particle mixture is set in motion by this fluid shear stress and the gravity. We only consider situations where this fluid shear stress is high enough to set a thick layer of sediment particles in motion (i.e., $\theta >> \theta_c$ and $\delta_s >> d_p$). The two layers, FL and SBL, are solved separately in the model. In the FL only the fluid phase momentum equation is solved. In the SBL a two-phase model is used with momentum equations for both fluid and particulate phases.

2.1. Two-Phase Model in the SBL Layer

[13] The present model is based on *Jackson*'s [2000] two-phase equations (1)–(4)

$$\frac{D\rho_f \varepsilon \overrightarrow{u^f}}{Dt} = -\overrightarrow{\nabla} P^f \bar{\bar{I}} + \overrightarrow{\nabla}.\bar{\bar{\tau^f}} + \overrightarrow{\nabla}.\bar{\bar{R^f}} + \epsilon\rho_f \overrightarrow{g} + n\overrightarrow{f}, \quad (1)$$

$$\frac{D\rho_p \phi \overrightarrow{u^p}}{Dt} = -\overrightarrow{\nabla} P^p \bar{\bar{I}} + \overrightarrow{\nabla}.\bar{\bar{\tau^p}} + \phi\rho_p \overrightarrow{g} - n\overrightarrow{f}, \quad (2)$$

$$\frac{D\epsilon}{Dt} = \frac{\partial \epsilon}{\partial t} + \overrightarrow{\nabla}.\left(\epsilon \overrightarrow{u^f}\right) = 0, \quad (3)$$

$$\frac{D\phi}{Dt} = \frac{\partial \phi}{\partial t} + \overrightarrow{\nabla}.\left(\phi \overrightarrow{u^p}\right) = 0, \quad (4)$$

in which ϵ and ϕ represent fluid and particles volume fractions. The other variables are defined, for a generic phase k, as follows: ρ_k represents the true density, $\overrightarrow{u^k}$

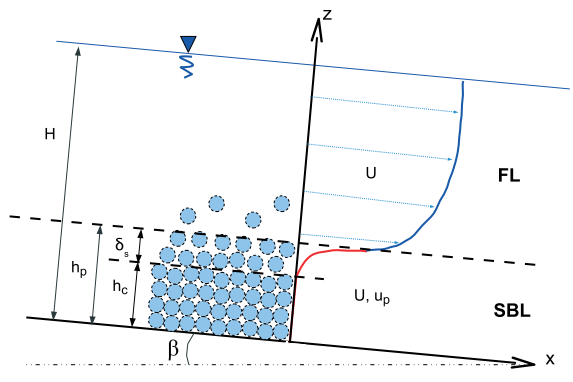

Figure 1. Sketch of unidirectional sheet flow.

corresponds to the volume averaged velocity, P^k is the pressure, $\bar{\bar{\tau}}^k$ represents the shear stress, where k stands either for the fluid phase f or the particulate phase p. $\bar{\bar{R}}^f$ corresponds to the fluid Reynolds stresses. The term $n\vec{f}$ represents the interactions between the fluid and the particulate phase and $\vec{g}$ classically corresponds to the gravitational acceleration.

[14] In this paper, we focus on a unidirectional and steady sheet flow, therefore, the two-phase equations (1)–(4) simplify with all dependencies in t, x, and y vanishing. Because we are interested in the steady state solution, we further assume that the vertical velocities of both phases vanish. Therefore, the mass conservation equation (3)–(4) are trivially satisfied. The variables that appear in the resulting equations are τ^f_{xz}, R^f_{xz}, ϵ, ϕ, P^{f}, P^{p}, nf_x, and nf_z, which only depend on the vertical upward direction z. The simplified system of equations reads

$$0 = \frac{d\tau^f_{xz}}{dz} + \frac{dR^f_{xz}}{dz} - nf_x + \epsilon\ \rho_f\ g\,sin\beta \tag{5}$$

$$0 = \frac{d\tau^p_{xz}}{dz} + nf_x + \phi\ \rho_p\ g\ sin\beta \tag{6}$$

$$0 = -\frac{dP^f}{dz} - nf_z - \epsilon\rho_f g\ cos\beta \tag{7}$$

$$0 = -\frac{dP^p}{dz} + nf_z - \phi\rho_p g\ cos\beta \tag{8}$$

$$\epsilon + \phi = 1 \tag{9}$$

[15] The system (5)–(9) is similar to the one proposed by *Ouriemi et al*. [2009] for the laminar case except for the presence of the term R^f_{xz} for the fluid Reynolds stresses.

2.1.1. Phases Interactions

[16] Following *Jackson* [2000], the terms nf_x and nf_z represent all the forces acting at the fluid-particle interface such as buoyancy, drag, lift, and Basset forces. In sediment transport problems, the dominant interaction forces are the buoyancy and the drag forces [*Hsu et al*., 2003, 2004; *Bombardelli and Jha*, 2009]. In the vertical direction the buoyancy force is the only interaction force at steady state

$$nf_z = -\phi\frac{dP^f}{dz}.$$

[17] In the horizontal direction, the fluid-particle interactions are the generalized buoyancy force, due to the fluid stresses acting on the fluid-particle interfaces, and the drag force induced by the velocity difference between the fluid and the particles

$$nf_x = \phi\frac{d\tau^f_{xz}}{dz} + C_D(U - u^p). \tag{10}$$

[18] In the second term of this relationship, C_{D} represents the drag coefficient. Following *Jenkins and Hanes* [1998] and *Hsu et al*. [2004], the Dallavalle formulae is used with *Richardson and Zaki*'s [1954] correction

$$C_D = \frac{\rho_f\phi}{d_p(1-\phi)^{3.1}}\left(0.3(U-u^p) + 18.3\frac{\eta_f}{\rho_f d_p}\right), \tag{11}$$

where $U = (1-\phi)u^{\mathrm{f}} + \phi u^{\mathrm{p}}$ represents the volume-averaged mixture velocity.

[19] Introducing the buoyancy force in the vertical momentum equations (7)–(8), a hydrostatic pressure distribution is obtained for both phases. This is consistent with *Berzi*'s [2011] analytical solution.

$$\frac{dP^f}{dz} = \rho_f g cos\beta \quad \text{and} \quad \frac{dP^p}{dz} = \phi\Big(\rho_p - \rho_f\Big)gcos\beta. \tag{12}$$

[20] Introducing the expression of nf_x (10) in the horizontal momentum equations (5)–(6) leads to the following system of equations:

$$0 = \frac{dR^f_{xz}}{dz} + \epsilon\frac{d\tau^f_{xz}}{dz} - C_D(U-u^p) + \epsilon\ \rho_f\ gsin\beta \tag{13}$$

$$0 = \frac{d\tau^p_{xz}}{dz} + \phi\frac{d\tau^f_{xz}}{dz} + C_D(U-u^p) + \phi\ \rho_p\ gsin\beta. \tag{14}$$

2.1.2. Closures of the Fluid Stresses

[21] Following the proposition of *Ouriemi et al*. [2009], a Newtonian form of the fluid phase viscous stresses is assumed

$$\tau^f_{xz} = \eta_e\frac{\mathrm{d}U}{\mathrm{d}z}, \tag{15}$$

where η_{e} is the effective viscosity. Because no theoretical model exists for dense suspension, *Ouriemi et al*. [2009] proposed to use the Einstein's viscosity $\eta_{\mathrm{e}}/\eta_{\mathrm{f}} = (1+5\phi/2)$. This choice was not definitely settled in this paper. Recently, *Boyer et al*. [2011] have measured the rheology of an isodense granular suspension in a pressure-controlled annular shear cell experiment. The authors have proposed the following relationship:

$$\frac{\eta_e}{\eta_f} = 1 + \frac{5}{2}\phi\left(1 - \frac{\phi}{\phi^m}\right)^{-1}, \tag{16}$$

which allows to recover Einstein's viscosity at low concentration, and diverges at the maximum packing fraction ϕ^{m} with a behavior similar to the Krieger-Dougherty formulation [*Krieger and Dougherty*, 1959].

[22] The fluid Reynolds stresses R^f_{xz} are closed using an eddy viscosity concept based on a mixing length approach

$$R^f_{xz} = \eta_t\frac{\mathrm{d}U}{\mathrm{d}z} \quad \text{with} \quad \eta_t = \rho_f(1-\phi)\ l_m^2\ \left|\frac{dU}{dz}\right|. \tag{17}$$

[23] The mixing length l_{m} is parameterized following *Li and Sawamoto* [1995] by

$$l_m = \kappa\int_0^z \frac{\phi^m - \phi}{\phi^m}\mathrm{d}z, \tag{18}$$

where κ is the Von Karman constant. This mixing length formulation has been used with some success by *Dong and*

Zhang [1999] in a two-phase model for oscillatory sheet flow. In this formulation, the mixing length is weighted by the integral of the concentration profile. Considering the limit case of a static bed at maximum volume fraction, the turbulence is fully damped in the bed and the classical linear Prandtl mixing length $l_m = \kappa(h_p - z)$ is recovered in a clear fluid boundary layer.

[24] The choice of a mixing length model is justified by the uniformity and the steadiness of the flow. Moreover, such a modeling for the fluid Reynolds stresses is coherent with the phenomenological approach for the intergranular stresses.

2.1.3. Closure of the Intergranular Stresses

[25] The intergranular stresses are modeled using the dense granular flows rheology $\mu(I)$ [*Forterre and Pouliquen*, 2008; *Boyer et al.*, 2011] in which the dimensionless number I can be interpreted as the ratio of a vertical time of rearrangement t_{micro} over a horizontal time of deformation $t_{\text{macro}} = ||\bar{\bar{\dot{\gamma}}}^p||^{-1} = |du^p/dz|^{-1}$

$$I = \frac{t_{micro}}{t_{macro}}.$$

[26] The microscopic time scale corresponds to the time needed by a particle submitted to a pressure P^p to fall over its own diameter. Following *Courrech du Pont et al.* [2003] and *Cassar et al.* [2005] three regimes can be observed: free fall, viscous, or turbulent. The corresponding time scales are given by

$$t^{ff}_{micro} = d_p\sqrt{\frac{\rho_p}{P^p}} \quad ; \quad t^{v}_{micro} = \frac{\eta_f}{P^p} \quad ; \quad t^{t}_{micro} = d_p\sqrt{\frac{\rho_f C_D}{P^p}}$$

[27] A phase diagram (Figure 2) can be drawn in the plane (St, r) where St is the Stokes number, defined as the ratio of the free fall time to the viscous one, and r is the ratio of the free-fall time to the turbulent one [*Cassar et al.*, 2005]. In the free-fall regime the fluid has no influence on the rheology and the granular media behaves like a dry granular flow. In the viscous regime, the vertical fall of a particle in the granular assembly is controlled by the viscous drag. In the turbulent regime, the vertical motion of the particle is controlled by the turbulent drag.

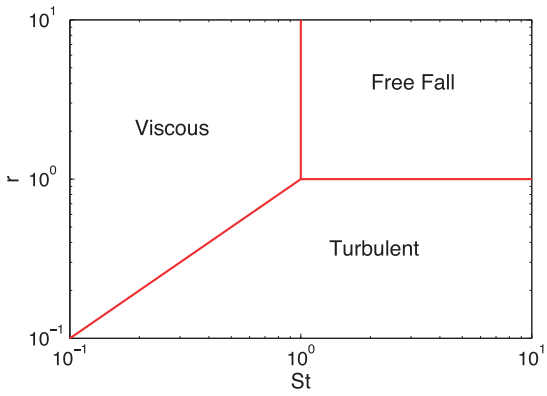

Figure 2. Phase diagram of the different flow regimes in the (St, r) plane for sheared immersed granular flows at imposed pressure [*Andreotti et al.*, 2011].

[28] A rough estimate of the characteristic time scales associated to the sheet flow regime gives the following values of the two above-mentioned dimensionless numbers $St \sim 10^{-2} - 10^2$ and $r \sim 10^{-2} - 10^1$ with typical particulate Reynolds number $Re_p = \rho_f w_s d_p/\eta_f \sim 10^{-1} - 10^2$, where w_s is the settling velocity of particles. The order of magnitudes used for these estimates are summarized in Table 1. These first estimates show that the granular flow is potentially at the transition between the three regimes. It is also possible that a transition occurs within the sheet flow layer itself.

[29] In the numerical model, the dimensionless number I is computed as the ratio of the largest microscopic time scales to the macroscopic one

$$I = \frac{\max\left(t^{ff}_{micro}, t^{v}_{micro}, t^{t}_{micro}\right)}{t_{macro}}.$$

[30] The dense granular flow regime is therefore obtained as a result of the model. This point will be discussed in detail in section 4.1.

[31] In the context of a frictional rheology, the particulate shear stress is written as

$$\tau^p_{xz} = \mu(I)P^p, \tag{19}$$

where the friction coefficient μ depends on the dimensionless number I as a result of the dimensional analysis. Following the idea originally introduced for dry granular flows [*GDR midi*, 2004; *Forterre and Pouliquen*, 2008], the same functional form has been used by *Boyer et al.* [2011] in the viscous regime

$$\mu(I) = \mu_s + \frac{\mu_2 - \mu_s}{I_0/I + 1}, \tag{20}$$

where μ_s corresponds to the static friction coefficient or the so-called tangent of the angle of repose, μ_2 represents a dynamical friction coefficient, and I_0 is an empirical parameter of the rheology.

[32] Following *Chauchat and Médale* [2010], a particulate viscosity is defined as

$$\eta_p = \frac{\tau^p_{xz}}{||\bar{\bar{\dot{\gamma}}}^p||} = \frac{\mu(I)P^p}{||\bar{\bar{\dot{\gamma}}}^p||}. \tag{21}$$

[33] It should be noted that the particulate viscosity diverges when the particulate shear rate $||\bar{\bar{\dot{\gamma}}}^p||$ vanishes. This is a typical characteristic of a viscoplastic behavior of which the archetype is the Bingham fluid model. The difference between the $\mu(I)$ rheology and the Bingham one lies in the dependency of the yield stress on the particulate pressure P^p. With this definition, if the particulate shear rate goes to zero, the particulate viscosity diverges and the granular media behaves like a solid material. In the numerical model, such divergence raises obvious numerical issues and a regularization technique [*Chauchat and Médale*, 2010] is used

$$\eta_p = \frac{\mu(I)P^p}{||\bar{\bar{\dot{\gamma}}}^p|| + \lambda}, \tag{22}$$

where λ is the regularization parameter. In the regularized problem, the solid behavior is replaced by a "very viscous"

Table 1. Order of Magnitudes for the Estimates of the Stokes (*St*), *r* Parameter and Particulate Reynolds Number ($\boldsymbol{Re_p}$) in the Sheet Flow Regime

Param.	ρ_p/ρ_f	$\rho_p - \rho_f$	ϕ	d_p	δ_s
Unit	(-)	$(kg \cdot m^{-3})$	(-)	(m)	(m)
O(•)	1	$10^2 - 10^3$	1	$10^{-4} - 10^{-3}$	$\sim 10\, d_p$

problem with a viscosity of order $O(\lambda^{-1})$. Consequently, a creeping flow is predicted by the model in the fixed sediment bed layer. It has been checked that for all the simulations presented herein, a value of the regularization parameter fixed to $\lambda = 10^{-6} s^{-1}$ guarantees a negligible creeping flow in the fixed bed layer ($z < h_c$).

2.1.4. Concentration Profile

[34] The prediction of the concentration profile is based on the dilatancy law $\phi(I)$ [*Forterre and Pouliquen*, 2008; *Boyer et al*., 2011]. *Boyer et al*. [2011] have measured precisely this relationship for volume fractions ranging from 0.4 to 0.585 in the viscous regime and have proposed the following relationship:

$$\phi(I) = \frac{\phi^m}{1 + I^{1/2}}. \tag{23}$$

[35] This formulation allows to describe the asymptotic behavior observed in the experiments $\phi^m - \phi \propto I^{1/2}$ close to ϕ^m and ensures the positivity of ϕ even for large values of I. It is also shown that this expression matches the experimental measurements from *Deboeuf et al*. [2009] down to $\phi = 0.3$ for the normal viscosity of dense suspension.

[36] From a physical point of view, two quantities control the dilatancy of the granular media: the particulate pressure and the shear rate. At constant particulate pressure, the concentration decreases when the shear rate increases. This mechanism can be responsible for the transition between the fixed sediment bed and the dilute suspension in sediment transport problems.

[37] In the present model, a similar relationship is used

$$\phi(I) = \frac{\phi^m}{1 + bI^{1/2}}, \tag{24}$$

where an additional parameter b, of order unity, has been introduced to allow calibration.

2.2. Boundary Layer Model in the FL

[38] In the FL the horizontal fluid momentum equation reduces to

$$0 = \frac{d\tau^f_{xz}}{dz} + \frac{dR^f_{xz}}{dz} + \rho_f \; g \; sin\beta, \tag{25}$$

where the presence of suspended particles is neglected both in the gravity and in the viscous stress terms. The closure for the fluid Reynolds stresses is identical to the SBL one (17)–(18). The mixing length at the bottom of the boundary layer is controlled by the concentration profile and the thickness in the moving SBL.

[39] In the turbulent boundary layer (FL), sediment particles can be suspended by the fluid turbulence. Following *Rouse* [1937], the suspended concentration profile is determined from a balance between the settling and the vertical turbulent dispersion fluxes of particles

$$w_s \phi + \frac{\eta_t}{\rho_f} \frac{d\phi}{dz} = 0, \tag{26}$$

where w_s represents the settling velocity of sediment particles. This balance equation can be integrated from a given vertical level at which the volume fraction is known up to the free surface H. Here the FL/SBL interface is chosen as the reference level.

$$\phi(z) = \phi_{h_p} \exp\left(-\rho_f w_s \int_{h_p}^{z} \eta_t^{-1} dz \right). \tag{27}$$

[40] The validity of the Rouse profile in the suspension above the sheet flow layer has been demonstrated by *Sumer et al*. [1996]. The authors have shown that the Rouse profile fit well their data provided that the reference level is taken high enough above the bed; it should lie in the upper half of the sheet flow layer, which corresponds to typical sediment concentration of order 0.25.

2.3. Resolution Strategy and Boundary Conditions

[41] For the numerical implementation, a pseudo time-integration and an implicit finite difference discretization technique are used to compute the steady state solution for both layers. The FL algebraic system is tridiagonal and is solved using a double sweep algorithm [*Thomas*, 1995] whereas the SBL two-phase algebraic system is solved using the Moore-Penrose solver of Matlab. The problem is decoupled between the two-layers FL and SBL as illustrated in Figure 3. The FL solution gives the bed shear stress applied on the SBL. In turn the SBL solution gives the boundary conditions for the FL: slip velocity U_b and sediment volume fraction at the interface ϕ_{h_p}. The mesh in the SBL is updated once after the FL solution to account for the sediment volume eroded from the SBL, and second at the end of the SBL solution, after the calculation of ϕ_{SBL} from equation (24). This latter step accounts for the bed decompaction. These two mesh adaptations lead to an error on the sediment volume conservation of less than 0.1 %. More details concerning the algorithm are given in Appendix B.

[42] No-slip boundary conditions are imposed for both velocities and the volume fraction is maximum at the bottom of the SBL (see Figure 3). The shear stress is imposed as boundary condition at the top of the FL (τ_{top} is zero for free-surface flows and is computed from the Colebrook and White formula for duct flows).

[43] At the end of the computations the model gives a prediction of the mixture velocity and the concentration profiles in the whole domain, from the fixed bed up to the

free surface, and the particulate phase velocity profile within the SBL. From this knowledge, the sediment transport rate $q_p = q_p^{\mathrm{FL}} + q_p^{\mathrm{SBL}}$ can be computed as

$$q_p^{FL} = \int_{h_p}^{H} \phi\ U\ dz \quad \text{and} \quad q_p^{SBL} = \int_{0}^{h_p} \phi\ u^p\ dz, \tag{28}$$

and the sheet flow layer thickness is computed as $\delta_s = h_p - h_c$. The lower limit of the mobile layer h_c is defined as the vertical position where the concentration has decreased 0.1% from the maximum packing fraction.

3. Results

[44] The proposed model is used to simulate sheet flow regimes involving two types of sediments over a large range of Shields numbers: $0.5 < \theta < 2.6$. Both sediment types are taken from sheet flow experiments presented in the literature [*Cowen et al.*, 2010; *Sumer et al.*, 1996] and cover a wide range of properties (Table 2).

[45] In section 3.1, we focus on the comparison of the vertical flow profiles with *Cowen et al.*'s [2010] and *Sumer et al.*'s [1996] experiments. Section 3.2 is dedicated to the study of the macroscopic parameters such as sediment transport rate, mobile layer thickness, and roughness.

3.1. Vertical Profiles

[46] At first, the model results are compared with two data sets from the literature [*Sumer et al.*, 1996; *Cowen et al.*, 2010] in terms of velocity and concentration profiles. The physical parameters for these simulations are summarized in Tables 2 and 3. The chosen values of the empirical parameters (κ, μ_2, I_0, and b) are given in Table 4.

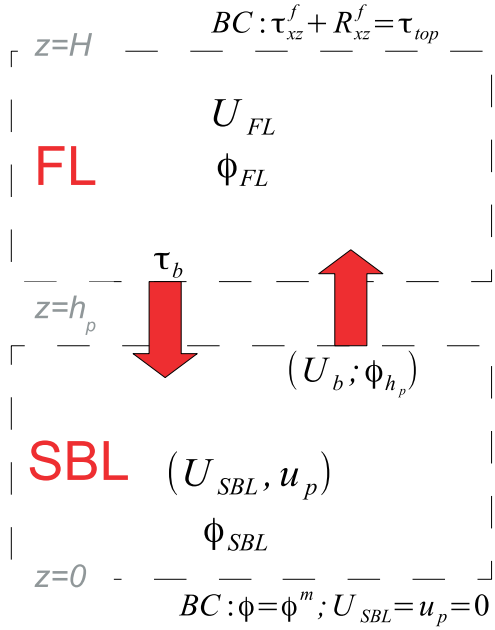

Figure 3. Sketch of the numerical resolution strategy.

[47] In the FL, the grid size is geometrically distributed with a reason of 1.048 and a minimum grid size taken as $\Delta z_{\min} = \min(0.1\eta_f/(\rho_f u_*); 0.1 d_p)$ resulting in N_{FL} grid points. In the SBL, the grid size is distributed following a cosine function refined at both boundaries. For all the simulations, the number of grid points N_{SBL} is fixed to 150, which leads to a minimum grid size smaller than d_p (see Table 4). The pseudo time step is fixed to 10^{-5} s. These numerical parameters ensure the spatial convergence of the numerical results.

[48] Figures 4a and 5a show the numerical velocity profiles compared with *Sumer et al.*'s [1996] and *Cowen et al.*'s [2010] measurements, respectively. In the four cases the simulated velocity profiles present a good agreement with experimental data for different experimental conditions and describe fairly well the transition from the static bed to the mobile sediment layer.

[49] In Figures 4b and 5b, concentration profiles for each experimental conditions are presented. The concentration profile in the SBL is calculated from the dilatancy law $\phi(I)$ (24) whereas it is obtained from the Rouse profile (27) in the FL. The value of the concentration at the top of the SBL is used as the boundary condition for the suspension solution in the FL. This value is in the range $\phi \in [0.2;0.3]$, which corresponds to the limit value below which the $\phi(I)$ law is valid [*Boyer et al.*, 2011] and above which the Rouse profile fits the experimental measurements [*Sumer et al.*, 1996].

[50] In *Sumer et al.*'s [1996] cases, the concentration profile in the dense part of the sheet layer was not measured. The present model results are compared with *Hsu et al.*'s [2004] results obtained with a two-phase model based on the kinetic theory for the intergranular stresses. It is interesting to note the similarity of the concentration profiles obtained with the dense granular flow rheology and the collisional theory [*Hsu et al.*, 2004]. In both cases the concentration profile exhibits a concentration "shoulder" of a few particles size thickness, characteristic of the existence of a sheet. Both phenomenological rheology and kinetic theory seem to be able to reproduce the existence of this sheet layer. Using γ-ray technique, *Pugh and Wilson* [1999] have measured concentration profiles in a cylindrical geometry that are consistent with the predicted profiles. However, more refined measurements are needed to improve our understanding of vertical dispersive mechanisms in the sheet flow layer.

[51] Concerning *Cowen et al.*'s [2010] experiment, the transition from the static bed to the sheet flow layer is smoother, but the concentration shoulder still exists. However, no experimental data or model results are available in the literature to further assess the predicted concentration profile. In the FL, the Rouse profile seems to match quite well with the concentration profile in the SBL.

Table 2. Sediment Properties for *Sumer et al.*'s [1996] (Type A) and *Cowen et al.*'s [2010] (Type B) Experiments

Sediment Type	Composition	Shape	d_p (mm)	ρ_p (kg/m^{-3})	ϕ_{max}	μ_s	w_s (m/s)
A	PMMA	Cylinders	2.6	1140	0.62	0.51	0.072
B	Glass	Beads	0.25	2600	0.6	0.3	0.0326

Table 3. Physical Parameters for the Simulations Corresponding to *Sumer et al.*'s [1996] and *Cowen et al.*'s [2010] Experiments

Parameters	Unit	*Cowen et al.* [2010]	*Sumer et al.* [1996] Run 82	*Sumer et al.* [1996] Run 91	*Sumer et al.* [1996] Run 99
Flow type		Free surface	Duct flow	Duct flow	Duct flow
Sediment type		B	A	A	A
θ		1.25	1.37	1.64	2.30
u_*	(m/s)	0.074	0.1	0.11	0.125
$sin\ \beta$		0.0035	0.00715	0.0086	0.0119
H	(cm)	12.5	17.4	17.5	17.6
h_p	(cm)	1.2	8.4	8.5	8.8
ρ_f	$(kg \cdot m^{-3})$	10^3	10^3	10^3	10^3
η_f	$(kg \cdot m^{-1} \cdot s^{-1})$	10^{-3}	10^{-3}	10^{-3}	10^{-3}

Table 4. Phenomenological and Numerical Parameters for the Simulations Corresponding to *Sumer et al.*'s [1996] and *Cowen et al.*'s [2010] Experiments. The Number in Brackets Refers to the Equation Containing the Parameter

	Sediment Type	κ (18)	μ_2 (20)	I_0 (20)	b (24)	N_{FL}/N_{SBL}
Sumer et al. [1996]	A	0.35	0.7	0.3	0.75	143/150
Cowen et al. [2010]	B	0.41	0.64	0.3	0.75	197/150

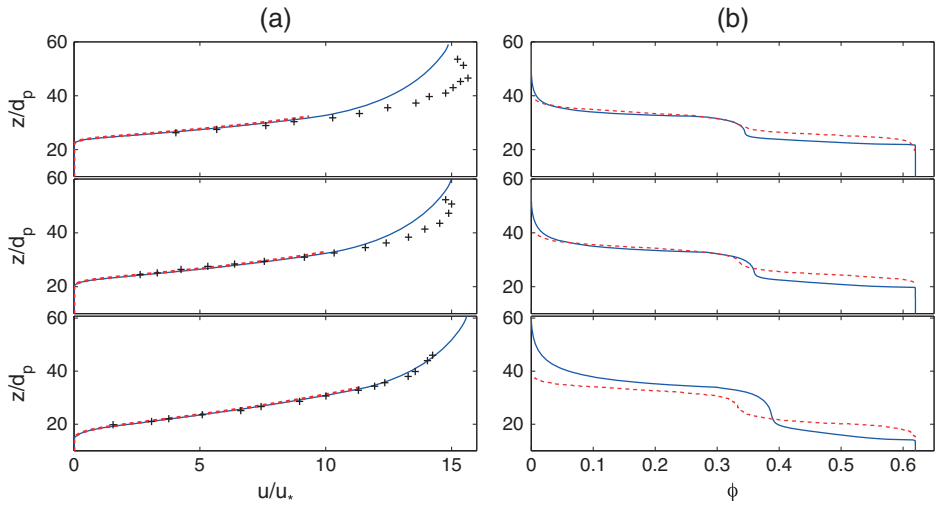

Figure 4. (a) Comparison of the fluid (blue line) and the particulate (red dashed line) velocity profiles between the present model and the measurements of *Sumer et al.* [1996] (plus), and (b) comparison of the concentration profiles predicted by the present model (blue line) with *Hsu et al.*'s [2004] results (red dashed line). From top to bottom, the left and right panels correspond to Run 82 ($\theta = 1.37$), Run 91 ($\theta = 1.65$), and Run 99 ($\theta = 2.3$) of *Sumer et al.*'s [1996] experiments.

As pointed out by *Sumer et al.* [1996], a Rouse profile matches the experimental measurements independently from the reference level chosen provided that the reference concentration is greater than approximately $\phi \approx 0.25$. This condition is quite well verified in the four cases presented here $\phi_{h_p} \in [0.25; 0.3]$. In the following, we will denote the concentration shoulder as the sheet layer.

[52] These first comparisons show that the proposed model is able to simulate quantitatively the velocity profiles and the concentration profiles for a wide range of Shields number ($\theta \in [1.25;2.3]$). It should be noted that the empirical constants of the phenomenological laws $\mu(I)/\phi(I)$, b, and I_0, are kept constant for both sediment types, A and B. In the four simulated cases, the concentration in the sheet layer is between $\phi = 0.3$ and $\phi = 0.4$, which is still in the validity domain of the phenomenological rheology [*Boyer et al.*, 2011]. The sensitivity of the model results to the empirical parameters κ, μ_2, I_0, and b will be discussed in section 4.2.

3.2. Macroscopic Parameters

[53] In this subsection, the macroscopic parameters predicted by the model are compared to experimental data and empirical

correlations from the literature in terms of sediment transport rate ψ, mobile layer thickness δ_s, and roughness k_s. Simulations have been performed, with the two sediment types A and B, for the following range of Shields number $\theta \in [0.5;2.6]$ by varying the bed slope at constant water depth.

[54] Figure 6 shows the comparison between the predicted dimensionless sediment transport rate ψ, the model results from *Hsu et al*. [2004], and the experimental data collected by *Yalin* [1977]. The total load ψ and the bed load contribution ψ^{SBL} are presented to exhibit the qualitative contribution of suspended load for each sediment type. The agreement between the model results and the experiments is rather good. For the light particles, type B, the contribution of the suspended load is much greater than the bed load one. On the contrary, for the massive particles, type A, the suspended load contribution is negligible compared to the bed load one. This observation is consistent with *Sumer et al*.'s [1996] phase diagram in the plane (θ, w_s/u_*). For sediment type A the ratio of the fall velocity over the friction velocity is in the range $w_s/u_* \in [0.74;1.7]$ whereas it is in the range $w_s/u_* \in [0.32;0.74]$ for sediment type B. Following *Sumer et al*.'s [1996] phase diagram, sediment type A simulations are mostly in the no suspension mode of sheet flow regime ($w_s/u_* > 1$), whereas sediment type B simulations are all in the suspension mode ($w_s/u_* < 0.8$). The present simulation results are consistent with these observations. It should be mentioned that our results are very close to *Hsu et al*.'s [2004] obtained with a two-phase approach based on kinetic theory of granular flows.

[55] Figure 7 shows the comparison between the dimensionless thickness computed with the present model δ_s/d_p, the model results from *Hsu et al*. [2004], and the experimental data reported by *Sumer et al*. [1996]. The comparison shows a fairly good agreement with experimental observations for both models especially for Shields numbers lower than 1.5. For higher Shields numbers, the evolution of the thickness predicted by our model presents a nonlinear behavior for sediment type A that is not observed in the measurements of *Sumer et al*. [1996] or *Hsu et al*. [2004] model results. It should also be pointed out that a significant scatter is observed on the *Sumer et al*. [1996] measurements

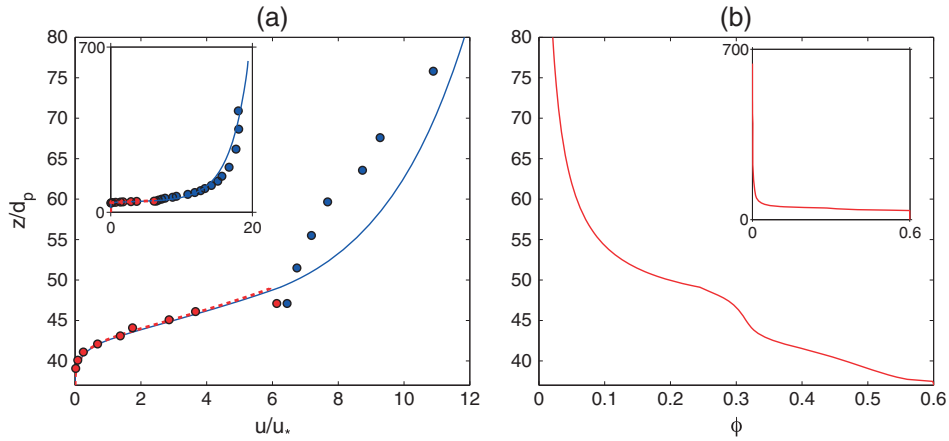

Figure 5. (a) Comparison of the fluid (blue line) and the particulate (red dashed line) velocity profiles between the present model and the measurements of *Cowen et al*. [2010], (red solid circle) and (blue solid circle). (b) The corresponding concentration profile.

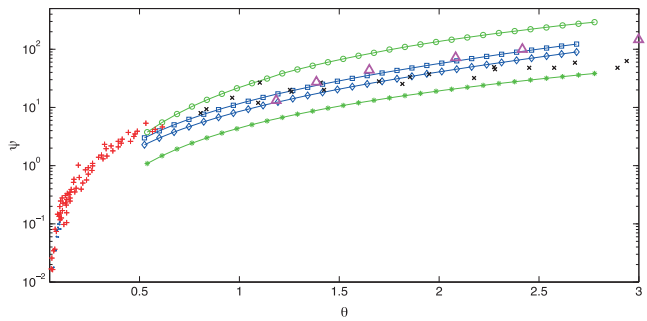

Figure 6. Dimensionless sediment transport rate $\psi = q_p/d_p\sqrt{(\rho_p - \rho_f)gd_p/\rho_f}$ and SBL contribution $\psi^{SBL} = q_p^{SBL}/d_p\sqrt{\rho_p g d_p/\rho_f}$ versus Shields parameter θ. Experimental data from *Meyer-Peter and Muller* [1948] (red, plus), *Wilson* [1966] (cross), *Gilbert* [1914] (blue, solid circle) synthesized in *Yalin* [1977]; model results from *Hsu et al*. [2004] (magenta, open triangle) ; total load and bed-load results from the present model for sediment type A (blue, open square; blue, open diamond), and type B (green, open circle; green, star), respectively.

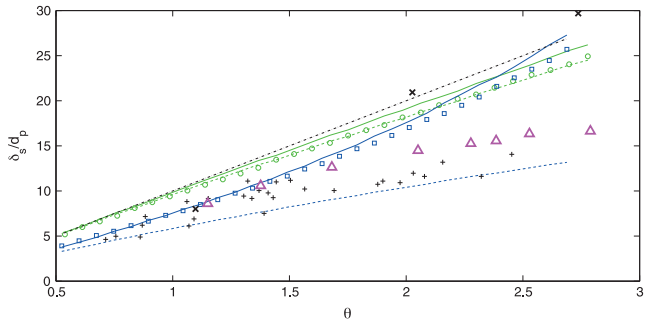

Figure 7. Comparison of the dimensionless sheet flow layer thickness $\boldsymbol{\delta_s/d_p = (h_p - h_c)/d_p}$ between the present model results for sediment types A: numerical solution (blue, open square), equation (32) (blue line), equation (33) (blue dashed line), and B: numerical solution (green, open circle), equation (32) (green line), equation (33) (green dashed line), model results from *Hsu et al.* [2004] (magenta, open triangle), *Wilson*'s [1987] model predictions (dash dotted line) and *Sumer et al.*'s [1996] data from visual observations (plus) and from concentration profiles (cross).

between visual observations and those deduced from concentration profiles (a factor of two for Shields number between 2 and 3).

[56] To better understand the influence of the particle properties (shape, density, and size), a simple model for the evolution of the thickness versus the Shields number is derived from the mixture momentum balance. This momentum balance is obtained as the sum of the momentum equations for the fluid and the particulate phases (13) and (14), respectively

$$0 = \frac{dR^f_{xz}}{dz} + \frac{d\tau^f_{xz}}{dz} + \frac{d\tau^p_{xz}}{dz} + \rho_m \ g \ \sin \ \beta, \tag{29}$$

where $\rho_\mathrm{m} = \epsilon \ \rho_\mathrm{f} + \phi\rho_\mathrm{p}$ is the mixture density. This equation can then be integrated between a given vertical position z in the SBL and the FL/SBL interface h_p, as follows:

$$R^f_{xz}(z) + \tau^f_{xz}(z) + \tau^p_{xz}(z) = \tau_b + g \sin\beta \int_z^{h_p} \rho_m(z)dz, \tag{30}$$

where it is assumed that the intergranular stresses vanishes at the FL/SBL interface $\tau^p_{xz}(h_p) = 0$ and $\tau_b = R^f_{xz}(h_p) + \tau^f_{xz}(h_p)$ represents the total fluid bed shear stress.

[57] We then introduce the mean sheet flow layer concentration $\bar{\phi}$, defined as: $\bar{\phi} \ \delta_s = \int_{h_c}^{h_p} \phi(z)dz$. Using this notation, the integral in the right-hand side of equation (30) can be rewritten as

$$\int_{h_c}^{h_p} \rho_m(z)dz = \delta_s\left[\rho_f + \left(\rho_p - \rho_f\right)\bar{\phi}\right]. \tag{31}$$

[58] Furthermore, at the location of the boundary between the stationary and moving sediment ($z = h_\mathrm{c}$), we can assume that the mixture stresses are dominated by the intergranular ones, i.e., the fluid stresses are negligible. This assumption will be justified in section 4.3. The velocity profiles presented in Figures 4 and 5 show that the shear rate goes to zero there. Consequently, the parameter I also vanishes and $\tau^p_{xz}(h_c) = \mu_s p^p(h_c)$, which is a classical Coulomb yield criterion [*Hanes and Inman*, 1985]. With these assumptions and the hydrostatic particulate pressure distribution (12), equation (30) can be rewritten between h_c and h_p in dimensionless form

$$\frac{\delta_s}{d_p} = \frac{\theta}{\mu_s \ \bar{\phi} \ \cos\beta - \left[\rho_f/\left(\rho_p - \rho_f\right) + \bar{\phi}\right]\sin\beta}. \tag{32}$$

[59] For sufficiently small inclination angles, i.e., $sin\beta \ll cos\beta \approx 1$, one obtains the following simple relationship for the thickness of the sheet flow layer:

$$\frac{\delta_s}{d_p} = \frac{\theta}{\mu_s\bar{\phi}}. \tag{33}$$

[60] These two last expressions are identical to equation (3.16) presented by *Ouriemi et al.* [2009] in the laminar case in which the longitudinal pressure gradient replaces the gravity term. The simplified model, equation (33), is similar to the one obtained by *Wilson* [1987], inspired from *Bagnold* [1956], with the difference that the friction coefficient here is the static one and not the dynamic one. In Figure 7, the predictions obtained with equations (32) and (33) together with the one from *Wilson*'s [1987] model are presented. For sediment types A and B, the predictions obtained using equation (32) are in good agreement with the full numerical solution. The slight overestimation of the dimensionless thickness, less than 5%, is induced by the regularization technique in a nontrivial way. Prediction obtained with (33) is a good approximation of (32) as far as the gravity term is negligible compared with the fluid bed shear stress and friction ones. This is the case for the "light particles" (type B) for which the proposed model and *Wilson*'s [1987] model are in good agreement. On the contrary, for the "massive particles" (type A) the gravity term is not negligible and a variation of as much as 100% is observed between the simplified model (33) and the complete one (32). One should keep in mind that gravity effects can become significant for "massive particles" that are not accounted for in simplified relationships such as (33) or *Wilson*'s [1987] model. For example, the simulations performed in this paper suggest that this is the case in *Sumer et al.*'s [1996] experiments.

[61] The difference between sediment type A and B shows an influence of the particle's frictional properties: sediment type A, which are not spherical, exhibits a higher static friction coefficient ($\mu_s = 0.51$) than the glass beads (sediment type B ; $\mu_s = 0.3$). This influence is captured by the simplified model (33); however, it is screened by the influence of gravity. Further works are needed to better understand the role of the particle properties in sheet flow regime (shape, size, and density).

[62] In Figure 8, the evolution of the dimensionless roughness versus the Shields number is presented. In the present model, the roughness is obtained from the value of the mixing length at the FL/SBL interface $k_s = l_m(h_p)$. This definition is consistent with our mixing length approach where its value at the interface represents the more energetic eddies length scale within the sheet flow layer. It is interesting to note that the roughness nondimensionalized by the thickness of the sheet layer is rather constant with the Shields number independently of the sediment types. This characteristic has been observed by *Grant and Madsen* [1982], *Nnadi and Wilson* [1992], and *Hsu et al*. [2004], among others, and is well reproduced by the present model.

[63] It appears from these three comparisons that the dense granular rheology allows to correctly predict the main features of the sheet flow regime.

4. Discussion

[64] In this section, the model results are analyzed and discussed. First, the dense granular rheology regime(s) encountered in the sheet flow regime are deduced from the model results. Second, the sensitivity of the model solution to the phenomenological parameters is presented. Third, the stresses repartition in the sheet flow layer are discussed and the vertical distribution of the sediment transport flux are analyzed. Finally, a discussion on the main limitations of both the kinetic theory of dense granular flows and the dense granular rheology for application to sheet flow regime is presented.

4.1. Dense Granular Rheology Regimes

[65] As mentioned in the model formulation (section 2), the sheet flow regime of sediment transport is at the transition between viscous, free fall, and turbulent regimes of the granular rheology. The phase diagram presented in Figure 2 allows to represents graphically these regimes. As explained previously, the competition between the three time scales associated with the vertical motion of a particle in the granular assembly leads to the three above-mentioned regimes:

- **Viscous regime**: $t^v_{micro} >> t^{ff}_{micro}$; t^t_{micro}.

i.e., $St << 1$ and $r >> St$

- **Free fall regime**: $t^{ff}_{micro} >> t^v_{micro}$; t^t_{micro}.

i.e., $St >> 1$ and $r >> 1$

- **Turbulent regime**: $t^t_{micro} >> t^v_{micro}$; t^{ff}_{micro}.

i.e., $St >> r$ and $r << 1$

[66] In Figure 9, the values of the Stokes number and the r number, for each grid point in the SBL and for all the simulations performed (i.e., for all Shields numbers), are plotted. As expected, most of the points are close to the transition. For all but a few points, the Stokes number is greater than unity, hence the particles' vertical motion is hardly affected by the fluid viscosity in the sheet flow regime. For the lighter particles most of the points are in the turbulent regime $r < 1 < St$ except at the FL/SBL interface. The particles' inertia does not control the vertical time scale of rearrangement for sediment type B and fluid turbulence is expected to be the control mechanism in the sheet flow layer. However, for sediment type A all the points are in the free fall regime; the grain inertia dominate the time scale of rearrangement, like in the dry granular case.

[67] *Ouriemi et al*. [2009], *Aussillous et al*. [2012], and *Boyer et al*. [2011] have shown that the $\mu(I)$ rheology is able to describe fairly well the granular flow in the viscous regime for different configurations. The agreement between the present model results and the experimental data from *Cowen et al*. [2010] (sediment type B) gives some clues that the granular rheology could be relevant in the turbulent regime as well. The authors are not aware of any publications concerning such application of the dense granular rheology in this regime.

[68] It is interesting to note that the predicted regimes of the dense granular rheology are consistent with the picture existing in the literature concerning the dominant mechanisms acting in the sheet flow regime: collisional interactions for massive particles, corresponding to the free fall regime,

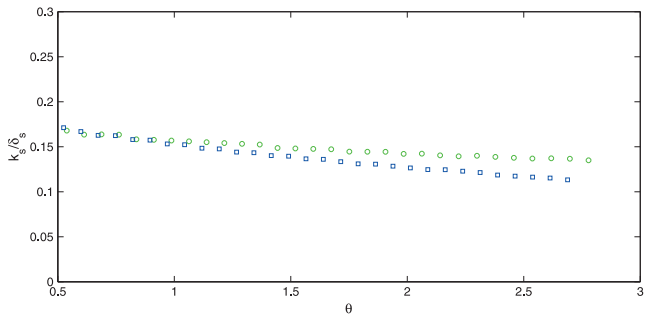

Figure 8. Dimensionless roughness k_s/δ_s versus Shields parameter θ for sediment types A (blue, open square) and B (green, open circle).

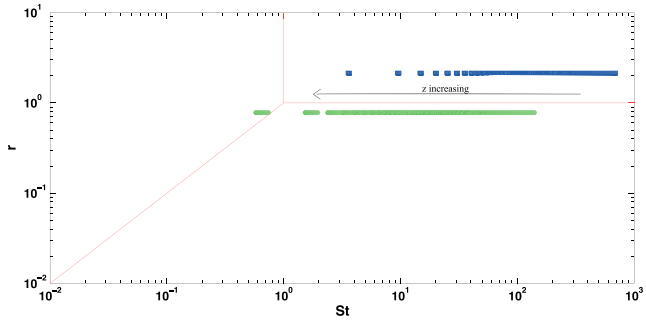

Figure 9. Phase diagram from *Andreotti et al.* [2011]. The limits in red (red line) represent $St = 1$, $r = 1$ and $St = r$. Local regimes for sediment A (blue, open square) and B (green, open circle). The arrow shows the equivalent variation of vertical position.

and fluid velocity fluctuations for light particles, corresponding to the turbulent regime. The phenomenological rheology seems to be able to capture intrinsically the transition between those two mechanisms.

4.2. Sensitivity Analysis

[69] The proposed model introduces several phenomenological parameters (κ, μ_2, I_0, and b, see Table 4). In the following, the chosen parameter values are discussed in light of previous works, and a sensitivity analysis for the two parameters I_0 and b is presented.

[70] The value of the Von Karman "constant" has been fixed to 0.35 for sediment type A, and 0.41 for sediment type B by comparison with experimental data. It has been suggested by *Vanoni* [1975] and *Amoudry et al.* [2008], among others, that the presence of sediment particles can lead to a reduction of the Von Karman constant. For example, *Longo* [2005] found values in the range 0.33 to 0.38 for sand sheet flows. To quantify the sensitivity to the Von Karman constant, we have performed simulations for *Sumer et al.*'s [1996] experiments with $\kappa = 0.41$, in place of 0.35, and have found relative variations of the sediment transport rate of 8%, 2.5%, and 2.3% for runs 82, 91, and 99, respectively. The relative variation for the sheet flow layer thickness is negligible (less than 1.5%). Therefore, the macroscopic parameters predicted by the model are not so sensitive to variations of the Von Karman constant.

[71] As stated in *Pouliquen* [1999] and [*Forterre and Pouliquen*, 2008], the parameter μ_2 is intrinsic to the particle type (material and shape) and corresponds to the tangent of the maximum angle below which a steady uniform flow is possible in gravity-driven flows down an inclined plane. From comparisons with experiments, we have calibrated $\mu_2 = 0.7$ for sediment type A and $\mu_2 = 0.64$ for sediment type B. These values are coherent with the ones presented in the literature [*Forterre and Pouliquen*, 2008; *Boyer et al.*, 2011].

[72] It follows that I_0 and b are the only two purely phenomenological parameters of the proposed model. The chosen value for I_0 is identical to the one used for dry granular flows in the inertial regime, e.g., *Forterre and Pouliquen* [2008]. In Figure 10 the sensitivity of the model results to the parameters I_0 and b is presented for the *Sumer et al.*'s [1996] experiments. Values of I_0 between 0.1 and 1 and b between 0.5 and 1 have been tested, and the relative variation of the dimensionless sediment transport rate $\Delta\psi/\psi^{\mathrm{ref}}$ and of the thickness $\Delta\delta_s/\delta_s^{\mathrm{ref}}$ are presented, where ψ^{ref} and δ_s^{ref} correspond to the reference results obtained with the original values of the parameters ($I_0 = 0.3$ and $b = 0.75$). It is observed that I_0 has no significant influence on the thickness ($\leq 5\,\%$), and the sediment transport rate shows maximum relative variation of 25 %. The parameter b has less influence on the sediment transport rate, with typical relative variations of about $\pm 15\,\%$ and more influence on δ_s than I_0 ($\approx \pm 15\,\%$). It is also observed that δ_s is an increasing function of I_0 and b whereas ψ is an increasing function of I_0 and a decreasing function of b. From this sensitivity analysis we can deduce that I_0, the phenomenological parameter of the $\mu(I)$ law, has mainly an influence on the velocity profile and not much on the concentration one. On the contrary, b, which only appears in the dilatancy law $\phi(I)$, has mainly an influence on the thickness. As a conclusion, the relatively small sensitivity of the model results to the phenomenological parameters, I_0 and b, demonstrates the robustness of the model.

4.3. Stresses and Sediment Flux Repartition

[73] Figure 11 shows the mixture stresses repartition in the SBL as given by (30). In the lower part of the sheet flow layer, where the concentration is close to the maximum packing fraction, the intergranular stresses dominate. Upper in the sheet flow layer, the intergranular stresses decrease and the fluid ones increase. At a given point, the fluid stresses and the intergranular ones match. This point is located around the two thirds of the sheet layer thickness. This was also observed by *Hsu et al.* [2004] in their two-phase model based on the kinetic theory of granular flows. In the concentration shoulder, both intergranular stresses and fluid Reynolds stresses are of the same order of magnitude. Above the concentration shoulder, the fluid Reynolds stresses dominate the mixture ones, consistently with the transition toward the suspension. In the whole domain, the relative contribution of the viscous stresses compared with the total fluid stresses are negligible except in a very thin layer near the bottom of the sheet flow layer. However, in this region the fluid stresses are negligible compared with the intergranular ones. Therefore, the contribution of the viscous stresses are not significant to this problem. This confirms the conclusion deduced from the analysis of the dense granular flow rheology regimes presented in section 4.1.

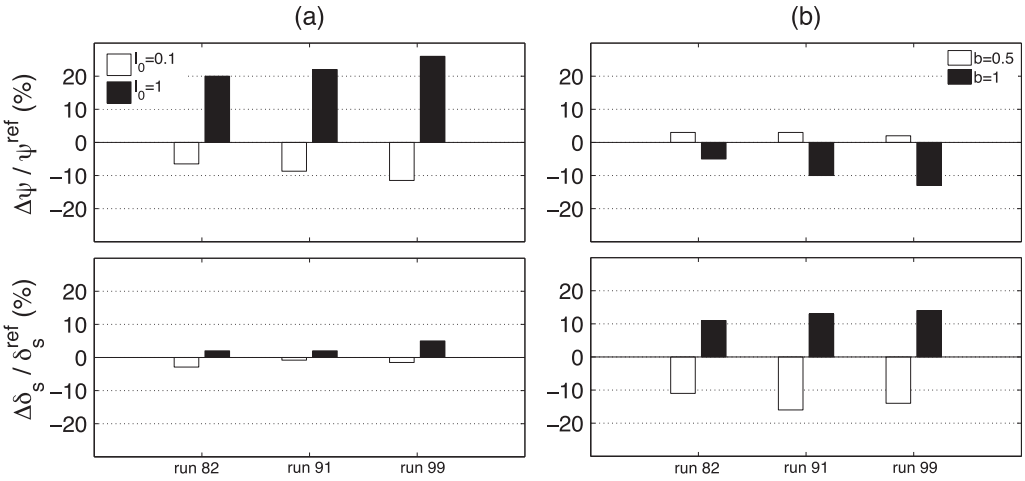

Figure 10. Sensitivity of the model results to the phenomenological parameters (a) I_0 and (b) b for the dimensionless sediment transport rate $\Delta\psi/\psi^{\mathrm{ref}}$ and the thickness of the sheet flow layer $\Delta\delta_s/\delta_s^{\mathrm{ref}}$. The values are relative to the reference simulation result (ψ^{ref}, δ_s^{ref}) obtained with $I_0 = 0.3$ and $b = 0.75$. The following values of the phenomenological parameters have been tested: $I_0 \in \{0.1;1\}$ and $b \in \{0.5;1\}$ for the three computed *Sumer et al.*'s [1996] runs.

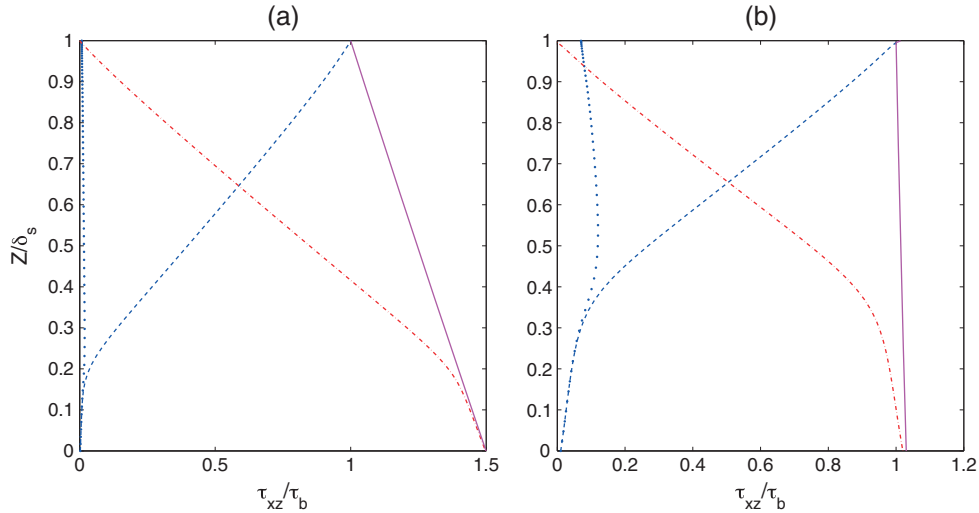

Figure 11. Results of the various contributions to the total mixture stresses inside the SBL, nondimensionalized by the shear stress at the interface SBL/FL (τ_b), for run 91 of (a) *Sumer et al.*'s [1996] and (b) *Cowen et al.*'s [2010] experiments. The vertical axis starts at the lower limit of the sheet and is nondimensionalized by the thickness. (magenta line) represents the mixture stresses, (red dash dotted line) represents the particulate stresses, (blue dashed line) represents the total fluid stresses, and (blue dotted line) represents the viscous contribution to fluid stresses.

[74] From a conceptual point of view, the SBL can be split into three layers: the upper layer, dominated by the fluid turbulence; the middle layer, corresponding to the concentration shoulder where the Reynolds stresses and the intergranular ones have the same order of magnitudes; and the lower layer, dominated by the particle-particle interactions. In *Berzi*'s [2011] model, a macroviscous layer is considered at the bottom where the fluid-particle mixture behaves as a viscous suspension. The collisional layer is split into two parts: a dense algebraic layer, in which an equilibrium between production of fluctuating energy and dissipation due to collisions is assumed, and a diffuse collisional layer, in which the balance of particle fluctuation energy is solved using the trapezium rule. The lower layer of the proposed model and the macroviscous one from *Berzi*'s [2011] model are physically consistent. However, in the collisional layer, *Berzi* [2011] neglects the fluid Reynolds stresses, whereas in the upper layer of the proposed model, the intergranular stresses are negligible. Therefore, improvements of both approaches requires a better understanding of the complex interactions between fluid turbulence and collisions (four-way coupling).

[75] It should also be pointed out that the concentration in this layer is obtained solely from the dilatancy law $\phi(I)$ and turbulent dispersion effects are neglected. Due to dominant fluid Reynolds stresses in the upper part of the SBL, this assumption is probably too strong. If this effect was accounted for, the concentration would be lower in this region and the concentration profiles would be closer to the ones predicted by *Hsu et al.*'s [2004] model (see Figure 4).

[76] The vertical distribution of the horizontal sediment flux $\pi = \phi u^p$ is presented in Figure 12 to determine the most efficient region for the sediment transport. The maximum of the flux is located at the SBL/FL interface ($\phi \approx 0.25 - 0.3$). The curves of the cumulative flux ($\Pi = \int_0^z \pi(\xi) d\xi$) show that different behaviors are observed for the two sediment types. With sediment type A [*Sumer et al.*, 1996], the sheet layer contributes to 65% of the total solid load, while for sediment type B [*Cowen et al.*, 2010], the sheet layer contributes only to 15% of the total solid load. As discussed in section 3.2, this is consistent with the phase diagram presented in *Sumer et al.* [1996]. The ratio of the fall velocity over the friction velocity controls the importance of the suspended load. Sediment type A has a ratio between 0.74 and 1.7, whereas sediment type B has a ratio between 0.32 and 0.74. Following *Sumer et al.* [1996], the transition between the no-suspension mode and the suspension mode of sheet flow is observed for a ratio lower than 0.8. Therefore, for "massive particles" ($w_s/u_* \geq 0.8$) ,the description of the SBL is critical to the prediction of the sediment transport flux. The dense granular rheology is shown to correctly predict the granular behavior in the sheet flow regime. For "light particles" ($w_s/u_* \leq 0.8$), the existence of a mobile sheet layer is associated to a high suspended load. It is essential to correctly describe the transition from the static bed to the suspension to get quantitative predictions of the sediment transport characteristics. The present model seems to be also relevant for this purpose; however, more precise validations against experimental data are needed.

4.4. Dense Granular Rheology Versus Kinetic Theory

[77] In this subsection, we discuss the limitations and advantages of both the kinetic theory and the dense granular rheology.

[78] Originally, the kinetic theory was developed to describe the gaseous regime of granular flows. It is based on the assumption of uncorrelated, instantaneous, and binary collisions [*Jenkins and Richman*, 1985] that are not verified when the particle response time is shorter than the fluid one (small Stokes number), and in dense shearing flows, when repeated collisions and/or enduring contacts between the particles occur [*Jenkins*, 2006, 2007].

[79] Concerning the influence of the ambient fluid, two mechanisms can modify the collisional interactions. First, when the particle inertia is so small that collisions are damped by the fluid viscosity [*Berzi*, 2011]. Second, when the particle response time is small compared with the fluid turbulent one the particles follow closely the fluid velocity fluctuations and the collisions cannot be considered as uncorrelated. *Hsu et al.* [2004] proposed a mixing length that depends on the Stokes number to account for this phenomenon.

[80] Mainly three approaches have been proposed to modify the original kinetic theory to account for enduring contacts [*Forterre and Pouliquen*, 2008, and references therein]. First, a frictional stress term can be added to the collisional one [e.g., *Johnson and Jackson*, 1987]. Second, the transport coefficients of the kinetic theory can be modified in the region of enduring contacts [e.g., *Kumaran*, 2006]. A last idea postulates the existence of a length scale larger than the particle diameter related to the formation of clusters [*Jenkins*, 2006]. To describe the transition between the gaseous and the liquid regimes, Hsu and coworkers [e.g., *Hsu et al.*, 2004] have introduced a modification of the radial distribution function and an additional closure for the particle pressure to account for enduring

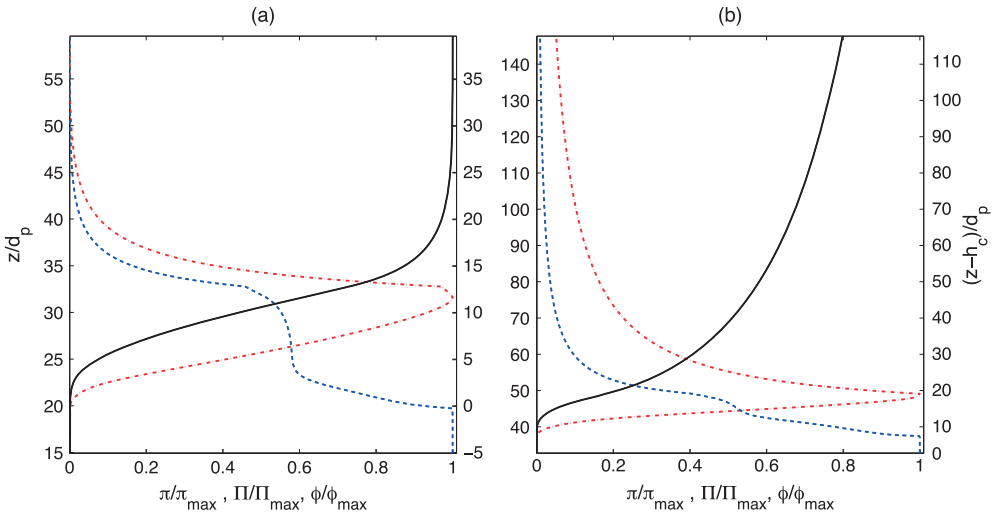

Figure 12. Concentration (blue dashed line), sediment flux (red dash dotted line) and cumulated sediment flux (black line) for (a) *Sumer et al.*'s [1996] experiment, run 91 ($\theta = 1.64$), and (b) *Cowen et al.*'s [2010] experiment ($\theta = 1.25$) with, respectively, $w_s/u_* = 0.94$ and $w_s/u_* = 0.44$.

contacts. *Berzi* [2011], in his analytical solution of sheet flow, has used the same approach to describe the liquid regime (macroviscous layer) and has accounted for multiple and repeated collisions using the correlation length proposed by Jenkins [e.g., *Jenkins*, 2006]. However, as stated by the authors, this extension is not meant to apply when enduring contacts dominate. It should also be noted that, in these models, the constitutive equations of the kinetic theory have been modified in a phenomenological way.

[81] Concerning the dense granular rheology, the following limitations apply to the modeling of sheet flow. First, no fundamental theory exists to link the form of the friction and dilatancy laws to the microscopic properties of the particles (e.g., restitution coefficient, shape, particle friction coefficient). Second, the hysteretic character of the flow threshold are not accounted for. Third, the phenomenological approach cannot capture the gaseous regime of granular flows. This regime falls in the framework of the kinetic theory. Besides that, the results presented in this paper show that the dense granular rheology coupled with the mixing length approach for the fluid Reynolds stresses allows to describe the sheet flow regime. Furthermore, as shown in the discussion on rheology regimes (section 4.1), the dense granular rheology potentially captures the transition between collisional dominant and fluid velocity fluctuations dominant sheet flow regime.

[82] From this short discussion, it appears clearly that both the kinetic theory and the phenomenological approach have some limitations concerning the modeling of sheet flow. The original kinetic theory is not appropriate in the dense part of the sheet flow, whereas the phenomenological approach is not appropriate for dilute conditions a priori. However, as illustrated in Figures 6 and 7, both approaches are shown to be able to quantitatively predict the main features of the sheet flow provided that constitutive laws are cautiously calibrated against experimental measurements. The proposed model can be considered as an alternative approach to the Bagnold's law and to the kinetic theory for modeling intergranular stresses. One of the advantages of the proposed model compared with kinetic theory ones is that no additional transport equations, with complex boundary conditions, have to be solved. However, some specific numerical techniques must be used to deal with the viscoplastic behavior of the dense granular rheology.

5. Summary and Conclusion

[83] An original two-phase model for sheet flow regime based on recent advances in dense granular flows has been presented. Using the dense granular rheology $\mu(I)$ and dilatancy law $\phi(I)$ coupled with a mixing length approach, the model has been validated against experimental data for the velocity profiles. The concentration profiles, for which no measurements are available, are consistent with those obtained by kinetic theory of granular flows. The evolution of the sheet flow macroscopic parameters such as sediment transport rate, thickness, and roughness, against Shields parameter are in good agreement with existing experimental data and empirical correlations.

[84] The main conclusions of the present paper can be summarized as follows:

1. The transition between collisional and fluid turbulent dominant sheet flow is captured by the dense granular rheology depending on the particles' characteristics and the local shear rate. This transition is characterized by a transition between the turbulent regime for "light particles", and the free fall one for "massive particles." In sheet flow regime, "massive particles" behave like a dry granular flow meaning that the fluid has a negligible influence on the particulate phase rheology.
2. The robustness of the model has been demonstrated from a sensitivity analysis performed for the two purely empirical parameters of the dense granular rheology (I_0 and b). For variations of these two parameters as high as 300%, the model solution only varies in a range of less than 25%.
3. A layer decomposition based on an analysis of the stresses repartition inside the sheet flow layer, is proposed:

(a) A dense frictional layer with dominant intergranular stresses that describes the transition to the static bed.
(b) A sheet layer where intergranular stresses and turbulent stresses are of the same order of magnitude.
(c) A turbulent dilute region with dominant turbulent stresses that describes the transition to the suspension.

4. From a practical point of view, the proposed model predicts a maximum of the sediment flux at the top of the sheet flow layer for both massive and light particles. For massive particles, most of the flux occurs in the moving bed layer, whereas for the light particles, most the flux occurs in the suspension layer.

[85] As a general conclusion, it has been demonstrated that the dense granular rheology ($\mu(I)/\phi(I)$) can be used as an alternative approach to the kinetic theory of granular flow for modeling intergranular stresses in the two-phase model for sheet flow regime.

[86] In a future work, a more refined turbulence model should be introduced to improve the modeling of the fluid-particle turbulent interactions (two-way and four-way coupling). Further works are also needed to better understand the influence of the particles' characteristics (shape, density, size, ...) on the dominant mechanisms acting in sheet flow regime. We strongly believe that higher-resolution experimental data inside the sheet flow layer are needed to further improve theoretical models.

Appendix A: Summary of the Model Equations

[87] The numerical model is based on the resolution of the following set of ordinary differential equations using an implicit finite difference method. The two layers are solved alternatively; the FL solution gives an estimate of the shear stress acting on the SBL whereas the FL solution gives an estimate of the slip velocity for the FL.

[88] **Boundary layer model in the FL**

$$0 = \frac{\mathrm{d}}{dz}\left[\left(\eta_f + \eta_t\right)\frac{du^f}{dz}\right] + \rho_f g \sin\beta \tag{A1}$$

[89] **Two-phase model in the SBL**

$$0 = \frac{\mathrm{d}}{\mathrm{d}z}\left[\eta_p \frac{du^p}{dz}\right] + \phi \frac{d}{dz}\left[\eta_e \frac{dU}{dz}\right] + C_D(U - u^p) + \phi \rho_p g \sin\beta \tag{A2}$$

$$0 = (1-\phi)\frac{d}{dz}\left[\eta_e \frac{dU}{dz}\right] + \frac{d}{dz}\left[\eta_t \frac{dU}{dz}\right] - C_D(U - u^p) + (1-\phi)\rho_f g \sin\beta \tag{A3}$$

$$\phi = \frac{\phi^m}{1 + b\ I^{1/2}} \tag{A4}$$

$$0 = +\frac{dP^f}{dz} + \rho_f g \cos\beta$$
$$0 = -\frac{dP^p}{dz} - \phi\left(\rho_p - \rho_f\right) g \cos\beta \tag{A5}$$

Appendix B: Numerical Algorithm [90]

Initialization : $k = 0$

$$U_{\mathrm{FL}}^0 = 0$$
$$U_{\mathrm{SBL}}^0 = 0; u^{p0} = 0 \text{ and } p^p = \phi^m \Delta\rho\ g\ \left(h_p - z^0\right)$$
$$\tau_b^{f0} = 0 \text{ and } U_b^0 = 0.$$

$k = k + 1$

Step 1: U_{FL}^{k+1} is obtained by solving (25) with bottom boundary conditions

$$(\eta + \eta_t)\frac{\mathrm{d}U_{SBL}^{k+1}}{\mathrm{d}z}\Big|_{z=H} = \tau_{fs}$$

and

$$U_{\mathrm{FL}}^{k+1}\big|_{z=h_p} = U_b^k$$

This solution gives the fluid bed shear stress $\tau_b^{f\ k+1}$.

Step 2: ϕ_{FL}^{k+1} is obtained from (27) and the suspended volume of sediment is given by

$$V_{\mathrm{FL}}^{k+1} = \int_{h_p^k}^{H} \phi_{FL}^{k+1} \mathrm{d}z.$$

Step 3: The space step in each cell is updated to ensure the total volume conservation

$$dz_j^* = dz_j^k + \frac{V_{\mathrm{FL}}^{k+1} - V_{FL}^k}{\phi_{SBL}^k (N_{SBL} - 1)}$$

The volume conservation reads

$$V_{FL}^{k+1} + V_{SBL}^* = V_{FL}^k + V_{SBL}^k$$

with $V_{SBL}^* = \int_0^{h_p^*} \phi_{SBL}^k dz$ and $V_{SBL}^k = \int_0^{h_p^k} \phi_{SBL}^k dz$.

Step 4: P^p the particulate pressure is updated after the remeshing of the SBL grid

$$P^p(z) = \Delta\rho g \int_z^{h_p^*} \phi_{\mathrm{SBL}}^k dz.$$

Step 5: U_{SBL}^{k+1} and u^{pk+1} are obtained by solving (13)–(14) with boundary conditions

$$(\eta + \eta_t)\frac{\mathrm{d}U_{SBL}^{k+1}}{\mathrm{d}z}\Big|_{z=h_p} = \tau_b^{f\ k+1}$$

and

$$U_{SBL}^{k+1}\Big|_{z=0} = u_{SBL}^{p\ k+1}|_{z=0} = 0.$$

This solution gives the value of the boundary condition in the FL: $U_b^{k+1} = U_{SBL}^k\big|_{z=h_p}$.

Step 6: ϕ_{SBL}^{k+1} is obtained from (24). This solution gives the value of the boundary condition in the FL $\phi_{h_p}^{k+1} = \phi_{SBL}^{k+1}\big|_{z=h_p}$.

Step 7: z^{k+1} is updated to ensure mass conservation in each cell j: $dz_j^{k+1}\phi_{SBLj}^{k+1} = dz_j^k \phi_{SBLj}^k$.

[91] This coupling procedure (step 1 to step 7) is iterated until convergence is reached for the two quantities τ_b^k and U_b^k with typical relative residual of 10^{-5}. Also, a convergence criteria of 10^{-6} on the relative residual for the velocities in root-mean-square norm is imposed for both layers. Step 3 ensures the mass conservation in the whole domain whereas step 7 ensures mass conservation in the SB layer due to the shear-induced decompaction of the sediment bed. A shear stress at the free surface τ_{fs} can be imposed to model the presence of a roof. It is calculated from the Colebrook and White formula.

[92] **Acknowledgments**. The authors acknowledge DGA for the financial support of the first author's Ph.D. Thesis (N° 2011-170914/DGA/DS/MRIS) and LEGI for its financial support. The authors also acknowledge P. Aussillous, Y. Forterre, E. Guazzelli, and O. Pouliquen for the fruitful discussions concerning the physics of dense granular flows and the phenomenological rheology, Daniel Lhuilier for the fruitful discussions concerning the two-phase model, and N. Delgado for the contribution to the model development during his Master's degree. The Associate Editor's and the two anonymous reviewers' constructive comments have been greatly appreciated during the review process.

References

Amoudry, L., T. J. Hsu, and P. L. F. Liu (2008), Two-phase model for sand transport in sheet flow regime, *J. Geophys. Res.*, *113*, C03011, doi:10.1029/2007JC004179.

Andreotti, B., Y. Forterre, and O. Pouliquen (2011), Les milieux granulaires entre fluide et solide, CNRS ed, p. 495, Paris.

Aussillous, P., J. Chauchat, M. Pailha, M. Médale, and E. Guazzelli (2012), Investigation of the mobile granular layer in bed-load transport, *J. Fluid Mech.*, Submitted.

Bagnold, R. A. (1954), Experiments on a gravity-free dispersion of large solid spheres in a newtonian fluid under shear, *Philos. Trans. R. Soc. London*, *225*, 49–63.

Bagnold, R. A. (1956), The flow of cohesionless grains in fluids, *Philos. Trans. R. Soc. London*, *249*, 235–297.

Berzi, D. (2011), Analytical solution of collisional sheet flows, *J. Hydraul. Eng.*, *137*(10), 1200–1207.

Bombardelli, F., and S. Jha (2009), Hierarchical modeling of the dilute transport of suspended sediment in open channels, *Environ. Fluid Mech.*, *9*, 207–235.

Boyer, F. m. c., E. Guazzelli, and O. Pouliquen (2011), Unifying suspension and granular rheology, *Phys. Rev. Lett.*, *107*, 188,301, doi:10.1103/PhysRevLett.107.188301.

Cassar, C., M. Nicolas, and O. Pouliquen (2005), Submarine granular flows down inclined planes, *Phys. Fluids*, *17*(10), 103301, doi:10.1063/1.2069864.

Chauchat, J., and M. Médale (2010), A 3D numerical model for incompressible two-phase flow of a granular bed submitted to a laminar shearing flow, *Comput. Meth. Appl. Mech. Eng.*, *199*, 439–449.

Courrech du Pont, S., P. Gondret, B. Perrin, and M. Rabaud (2003), Granular avalanches in fluids, *Phys. Rev. Lett.*, *90*, 044,301.

Cowen, E. A., R. D. Dudley, Q. Liao, E. A. Variano, and P. L.-F. Liu (2010), An insitu borescopic quantitative imaging profiler for the measurement of high concentration sediment velocity, *Exp. Fluids*, *49*(1), 77–88.

Deboeuf, A., G. Gauthier, J. Martin, Y. Yurkovetsky, and J. F. Morris (2009), Particle pressure in a sheared suspension: A bridge from osmosis to granular dilatancy, *Phys. Rev. Lett.*, *102*, 108,301, doi:10.1103/PhysRevLett.102.108301.

Dong, P., and K. Zhang (1999), Two-phase flow modelling of sediment motions in oscillatory sheet flow, *Coastal Eng.*, *36*(2), 87–109, doi:10.1016/S0378-3839(98)00052-0.

Forterre, Y., and O. Pouliquen (2008), Flows of dense granular media, *Annu. Rev. Fluid Mech.*, *40*, 1–24, doi:10.1146/annurev.fluid.40.111406.102142.

Gao, P. (2008), Transition between two bed-load transport regimes: Saltation and sheet flow, *J. Hydraul. Eng.*, *134*(3), 340–349.

GDR midi (2004), On dense granular flows, *Eur. Phys. J. E*, *14*, 341–365.

Gilbert, G. K. (1914), The transportation of debris by running water, *Tech. Rep*. *86*, USGS Professional Paper.

Grant, W. D., and O. S. Madsen (1982), Movable bed roughness in unsteady oscillatory flow, *J. Geophys. Res.*, *87*(C1), 469–481.

Greimann, B., and F. Holly (2001), Two-phase flow analysis of concentration profile, *J. Hydraul. Eng.- ASCE*, *127*, 753–761.

Hanes, D. M., and A. J. Bowen (1985), A granular-fluid model for steady intense bed-load transport, *J. Geophys. Res.*, *90*.

Hanes, D. M., and D. L. Inman (1985), Experimental evaluation of a dynamic yield criterion for granular fluid flows, *J. Geophys. Res.*, *90*(B5), 3670–3674.

Hsu, T., J. T. Jenkins, and L. F. Liu (2003), On two-phase sediment transport: Dilute flow, *J. Geophys. Res.*, *108*, 14.

Hsu, T.-J., J. T. Jenkins, and P. L.-F. Liu (2004), On two-phase sediment transport: sheet flow of massive particles, *P. Roy. Soc. Lond. A. Math.*, *460*(2048), 2223–2250, doi:10.1098/rspa.2003.1273.

Jackson, R. (2000), The Dynamics of Fluidized Particles, pp. 17–64, Cambridge University Press, Cambridge.

Jenkins, J. T. (2006), Dense shearing flow of inelastic disks, *Phys. Fluids*, *18*, 393–410, doi:10.1063/1.2364168.

Jenkins, J. T. (2007), Dense inclined flow of inelastic spheres, *Granular matter*, *10*, 47–52, doi:10.1007/s10035-007-0057-z.

Jenkins, J. T., and D. M. Hanes (1998), Collisional sheet flows of sediment driven by a turbulent fluid, *J. Fluid Mech.*, *370*(1), 29–52, doi:null.

Jenkins, J. T., and M. W. Richman (1985), Grad's 13-moment system for a dense gas of inelastic spheres, *Arch. Ration. Mech. Anal.*, *87*, 355–377.

Johnson, P. C., and R. Jackson (1987), Frictional-collisional constitutive relations for granular materials, with application to plane shearing, *J. Fluid Mech.*, *176*, 67–93.

Krieger, I. M., and T. J. Dougherty (1959), A mechanism for non-Newtonian flow in suspensions of rigid spheres, *Trans. Soc. Rheol.*, *3*, 137–157.

Kumaran, V. (2006), The constitutive relation for the granular flow of rough particles, and its application to the flow down an inclined plane, *J. Fluid Mech.*, *561*, 1–42.

Li, L., and M. Sawamoto (1995), Multi-phase model on sediment transport in sheet-flow regime under oscillatory flow, *Coastal Eng. Jpn.*, *38*, 157–178.

Longo, S. (2005), Two-phase flow modeling of sediment motion in sheet-flows above plane beds, *J. Hydraul. Eng.*, *131*(5), 366–379, doi:10.1061/(ASCE)0733-9429(2005)131:5(366).

Meyer-Peter, E., and R. Muller (1948), Formulas for bed-load transport, in 2nd Meeting of the International Association of Hydraulic and Structural Research, pp. 34–64.

Nnadi, F. N., and K. C. Wilson (1992), Motion of contact-load particles at high shear stress, *J. Hydraul. Eng.*, *118*(12), 1670–1684, doi:10.1061/(ASCE)0733-9429(1992)118:12(1670).

Ouriemi, M., P. Aussillous, and E. Guazzelli (2009), Sediment dynamics. Part I: Bed-load transport by shearing flows, *J. Fluid Mech.*, *636*, 295–319.

Pouliquen, O. (1999), Scaling laws in granular flows down rough inclined planes, *Phys. Fluids*, *11*(3), 542–548, doi:10.1063/1.869928.

Pugh, F. J., and K. C. Wilson (1999), Velocity and concentration distributions in sheet flow above plane beds, *J. Hydraul. Eng.*, *125*(2), 117–125.

Richardson, J. F., and W. N. Zaki (1954), Sedimentation and fluidization: Part i, *Trans. Inst. Chem. Eng.*, *32*, 35–53.

Rouse, H. (1937), Modern conceptions of the mechanics of turbulence, *Trans. Am. Soc. Civ. Eng.*, *102*, 463–505.

Sumer, B. M., A. Kozakiewicz, J. Fredsøe, and R. Deigaard (1996), Velocity and concentration profiles in sheet-flow layer of movable bed, *J. Hydraul. Eng.*, *122*(10), 549–558, doi:10.1061/(ASCE)0733-9429(1996)122:10(549).

Thomas, J. W. (1995), Numerical Partial Differential Equations : Finite Difference Methods, 437 pp., Springer, New York.

Vanoni, V. A. (1975), Sedimentation engineering, Manual 54, *Am. Soc. Coastal Eng.*, New York, 745 p.

Wilson, K. (1987), Analysis of bed-load motion at high shear stress, *J. Hydraul. Eng.*, *113*, 97103.

Wilson, K. C. (1966), Bed-load transport at high shear stress, in Proc. A.S. C.E, vol. *HY6*, ASCE.

Wilson, K. C. (1989), Mobile-bed friction at high shear stress, *J.Hydraul. Eng.*, *115*(6), 825–830, doi:10.1061/(ASCE)0733-9429(1989)115:6(825).

Yalin, M. S. (1977), Mechanics of sediment transport, 2nd ed., 141 pp., Pergamon Press, Ontario.